ELSEVIER

Catalysis Today 33 (1997) 119–137

CATALYSIS TODAY

Catalytic properties of MoO_3 revisited

Jerzy Haber *, Erwin Lalik

Institute of Catalysis and Surface Chemistry, Polish Academy of Sciences, ul. Niezapominajek 1, 30-239 Kraków, Poland

Abstract

One of the most striking features of molybdenum oxide is the versatility of its catalytic properties, which are determined by the valence state of molybdenum ions and their local environment. It may be anticipated that MoO_3 surface must contain catalytic sites which are active in different types of elementary steps. Different probe catalytic reactions were thus applied to monitor the changes of the concentrations of various types of active sites in the course of the reduction of MoO_3 to MoO_2 and to unravel their role in the complex reaction network of such molecule as butene. Isomerization of 3,3-dimethylbutene-1 was used to characterize Brønsted acid sites, the ability of the MoO_3 surface to generate allylic species was determined by the isomerization of 2,3-dimethylbutene-2. The presence of sites inserting oxygen into the hydrocarbon molecule was identified by the reaction of allyl iodide to form acrolein. Dehydrogenation of butene-1 to butadiene was applied as the test reaction to detect sites responsible for abstraction of β hydrogen. Total oxidation was taken as a measure of the concentration of sites adsorbing electrophilic oxygen. The nature of different sites is discussed.

Keywords: Molybdenum; Catalytic properties

1. Introduction

One of the most striking features of molybdenum oxide is the versatility of its catalytic properties [1]. Molybdenum oxide-based catalysts are active and selective in many reactions belonging to very different types such as reactions with the participation of hydrogen or oxygen, which may be considered as redox processes, as well as isomerization, addition or decomposition, which are usually classified as acid–base processes. Parameters which determine the catalytic behaviour of molybdenum oxides are the valence state of molybdenum ions, their local environment and the type of crystal plane, on which they are exposed. It may thus be anticipated that MoO_3 surface must contain catalytically active sites which are active in different types of elementary steps.

When an olefin is brought in to contact with a MoO_3 surface, a complex reaction network may develop, as illustrated in Fig. 1 for the case of butene [2]. An olefin molecule begins to interact with the surface by forming weak hydrogen bonds with the surface OH groups. These groups show Brønsted acid properties strong enough for the transfer of a proton from the surface to the olefin to take place resulting in the formation of a carbocation. This may start the whole network of reactions proceeding by the carbocation mechanism, like isomerization, cracking, etc.

* Corresponding author.

PII S0920-5861(96)00107-1

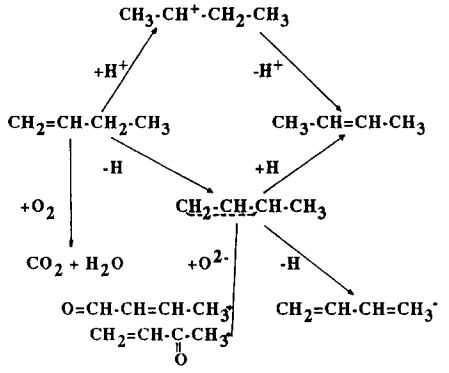

Fig. 1. Reaction network of butene-1 on MoO_3 catalyst.

The π bond of the olefin, instead of interacting with a surface proton, may react with an empty orbital of molybdenum and form a surface π-complex. Polarized Mo–O bonds on (100) and (101) crystal planes can readily interact with C–H bond in the α position of the olefin which results in the abstraction of hydrogen and formation of an allylic species. The surface oxygen ions O^{2-} on the (010) plane, bridging the MoO_6 octahedra, which are characterized by strong basic properties [3] may perform a nucleophilic attack on the allyl leading to the formation of an aldehyde in case of an attack on the primary carbon atom or ketone in case of the secondary one. The question of the role of different crystal planes of MoO_3 in the oxidation of hydrocarbons has been in recent years a subject of a lively discussion [4–9].

It may be thus concluded that MoO_3 surface must contain catalytically active sites which participate in at least five types of elementary steps:

(i) isomerization of olefins through the formation of carbocations,

(ii) abstraction of a hydrogen to form allylic species,

(iii) abstraction of the second hydrogen resulting in the formation of diene,

(iv) nucleophilic addition of oxygen to the allyl to form oxygenated precursor (aldehyde or ketone),

(v) generation of electrophilic oxygen species O^-, O_2^- or O_2^* which are involved in total oxidation of the organic molecule to CO_2.

It could be anticipated that the relative surface concentrations of these sites should be strongly dependent on the degree of reduction of the oxide. It seemed therefore of interest to apply different probe catalytic reactions to monitor the changes of the concentrations of different types of active sites in the course of the reduction of MoO_3 and to unravel their role in a complex reaction network of such molecules as, for example, butene.

2. Experimental

2.1. Materials

MoO_3 supplied by Climax Molybdenum Co. was prior to the experiments calcined at 500°C for 5 h in air. Its surface area, determined by the BET method from low temperature krypton adsorption, was 2.59 $m^2\ g^{-1}$. It was a powder material composed of small crystallites approximately spherical in shape. The Bi-doped catalyst was prepared by impregnation of MoO_3 in the aqueous bismuth nitrate solution. The impregnation did not cause any changes of morphology or surface area. Propene, butenes, 3,3-dimethylbutene-1 (3,3-DMB-1), 2,3-dimethylbutene-2 (2,3-DMB-2) were supplied by Fluka (purum), allyl iodide by Merck.

2.2. Techniques

2.2.1. X-ray diffraction

The X-ray powder diffraction (XRD) investigations were carried out with the DRON-2 diffractometer using $\lambda = 0.15405$ nm radiation.

2.2.2. IR spectroscopy

IR transmission spectra were obtained with a SPECORD M-80 spectrometer using pellets containing 1.5 mg of the sample in 800 mg of KBr.

2.2.3. X-ray photoelectron spectroscopy

X-ray photoelectron spectra were recorded with a VG ESCA 3 apparatus using monochromatic Al K_α radiation with an energy of 1486.6 eV. Specimens were taken out from the catalytic reactor and deposited on a copper holder from an acetone suspension or by powdering onto adhesive tape. The measurements were carried out at a temperature of 25°C and a pressure of 10^{-6} Torr. The values of binding energies were calibrated against the C1s line assumed to correspond to 285 eV.

2.2.4. Determination of catalytic activity

Catalytic experiments were carried out in a stainless steel pulse microreactor connected with the gas chromatograph through a four-way valve enabling the products to be directed into one of two columns. The first one, 4 m long with DMS served for the separation of gaseous products for analysis with a catharometer, the second one, 2 m long with silica oil DC-550 on Chromosorb G was used for the determination of liquid products with a FID. After each pulse one type of products could be analysed, each experimental point required thus two pulses to be passed through the reactor. In the case of experiments with 3,3-dimethylbutene-1 the glass reactor was applied. The sample of the catalyst was 0.5 g. Helium was used as the carrier gas at a flow rate of 30 cm^3 min^{-1}. In some cases it was not possible to obtain a full carbon balance due to the deposition of coke, but this did not have any bearing upon the conclusions. The yield was calculated as the ratio of the amount of the given product formed (in moles) to the amount of reagent introduced (in moles) expressed in %, after taking into account the stoichiometric coefficients.

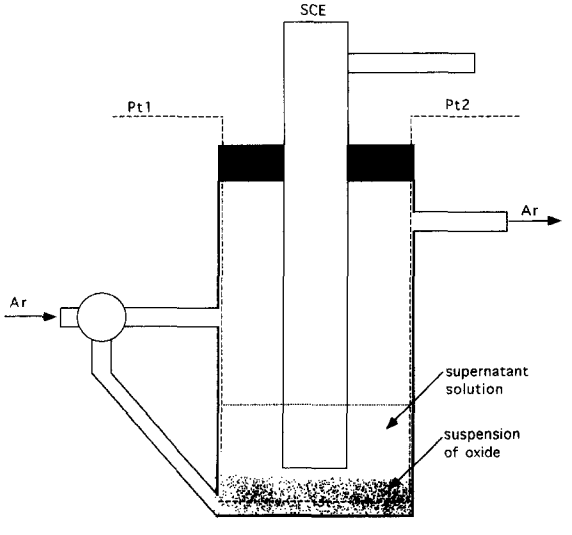

Fig. 2. The set-up for the determination of MoO_3/MoO_2 powder electrode potential.

2.2.5. Determination of the potential of powder MoO_3/MoO_2 electrode

The bottom of the cell shown in Fig. 2 was filled with 0.1 g of mixture of MoO_3 and MoO_2 taken in different ratios, or with the catalysts in different stages of the reduction, and covered with 2 ml of water. The cell was quipped with two platinum electrodes: Pt1 immersed in the aqueous phase about 1 cm above the bottom and Pt2 inserted into the powder, and the standard calomel electrode (SCE). The flow of argon was passed for 1 h from the bottom of the cell to obtain a good suspension of the powder in water. It was then switched to the volume above the solution and the potentials of the platinum electrodes Pt1 and Pt2 against SCE were recorded for several hours.

3. Results

3.1. Reactions of butene-1

Fig. 3a shows the selectivities to different products observed when successive pulses of butene-1 in oxygen-free helium were passed over the MoO_3 catalyst at 440°C. Thus, the curves represent the changes of selectivity to a given product versus degree of reduction x in the formula MoO_{3-x}. It may be seen that at the beginning of the experiment, when pure MoO_3 is present in the reactor, *cis* + *trans* butene-2 and butadiene are the main products, only small

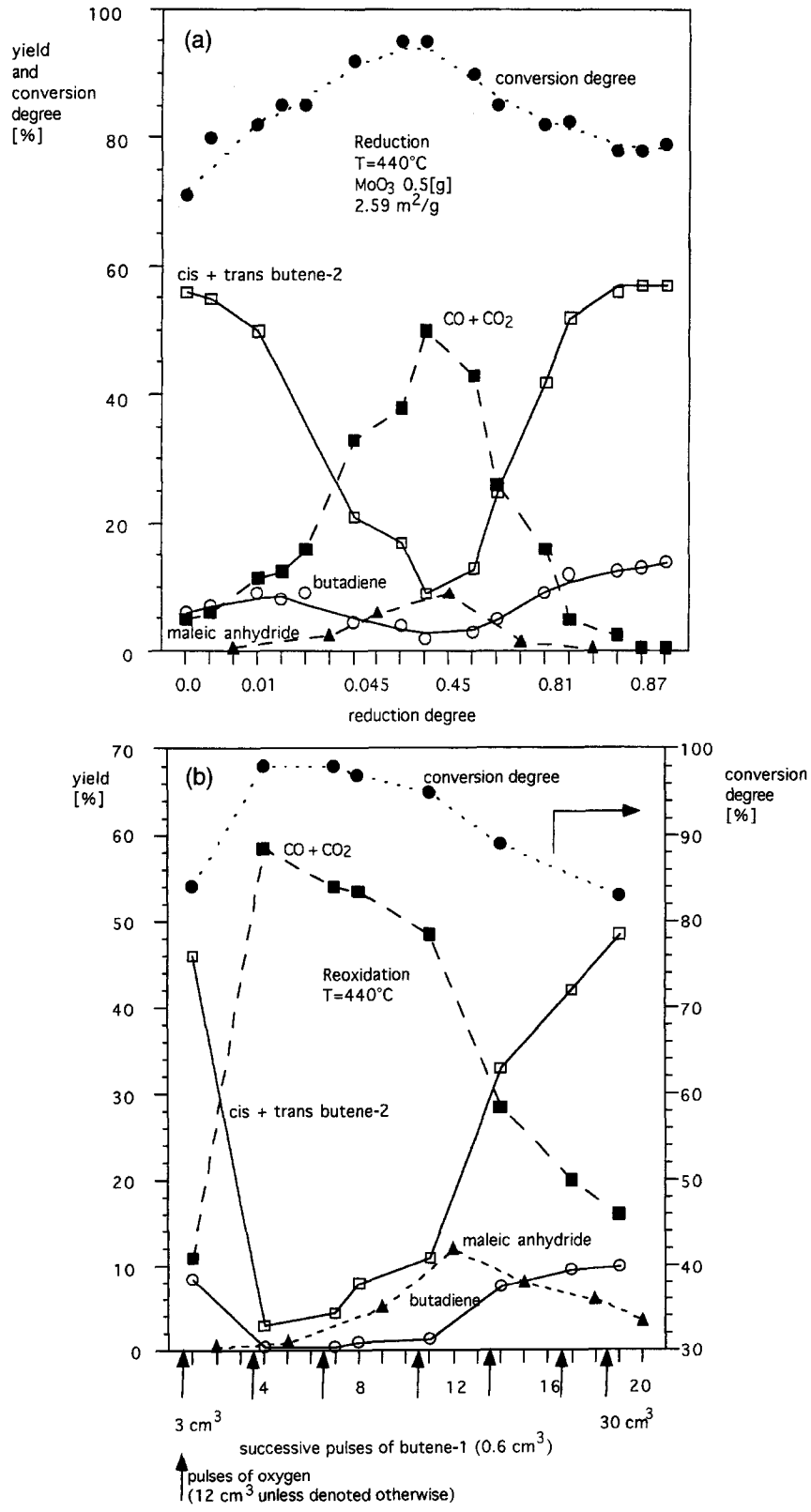
(a)
yield and conversion degree [%]
conversion degree
Reduction
T=440°C
MoO3 0.5[g]
2.59 m2/g
cis + trans butene-2
CO + CO2
butadiene
maleic anhydride
reduction degree
(b)
yield [%]
conversion degree [%]
Reoxidation
T=440°C
successive pulses of butene-1 (0.6 cm3)
pulses of oxygen
(12 cm3 unless denoted otherwise)

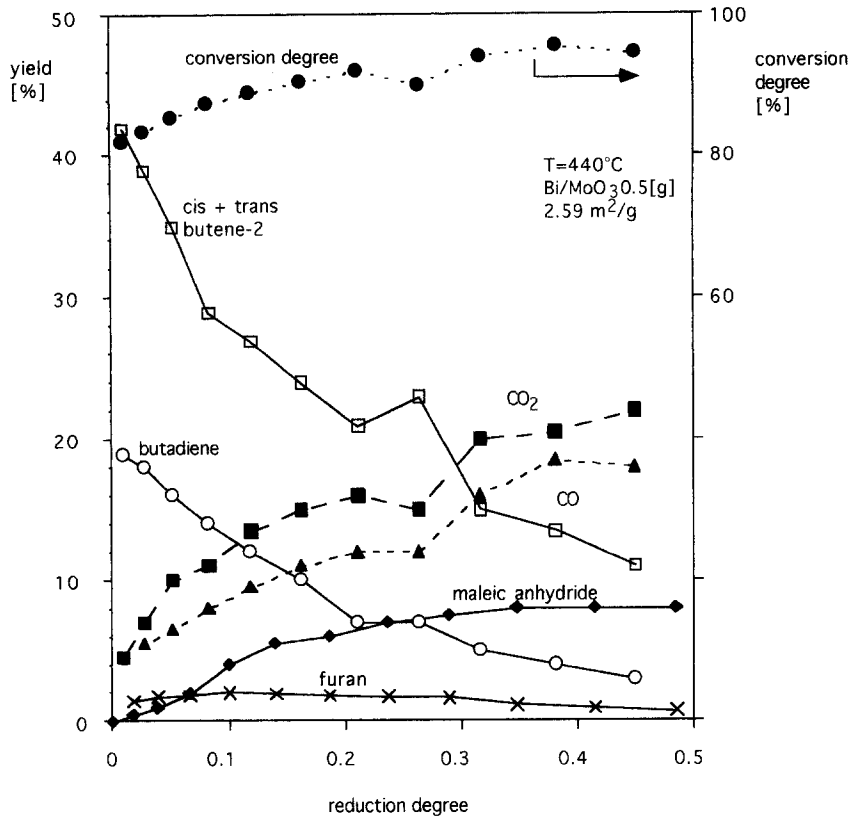

Fig. 4. Conversion of butene-1 and yields of products as a function of reduction degree of Bi^{3+}/MoO_3 catalyst.

amounts of maleic anhydride and CO_x being formed. As the degree of reduction increases, the selectivities to butene-2 and butadiene decrease whereas those to maleic anhydride, CO and CO_2 as well as total conversion rise. A characteristic point is reached, in which the yields of butene-2 and butadiene attain minimum, whereas the yields of maleic anhydride and $CO + CO_2$ – a maximum, and on further reduction selectivities change in opposite direction, volcano-shaped symmetrical curves being obtained. Similar results were obtained when between the pulses of butene-1 hydrogen was passed at 480°C to reduce MoO_3, or when pulses containing a mixture of butene-1 and oxygen (in the ratio of 1:2) were injected instead of pure butene-1. It may be thus concluded that the change of reactivity pattern of MoO_3 is independent of the type of reducing agent used for its reduction or the presence of oxygen.

If the main factor determining the selectivities to different products were the degree of reduction of the surface prevailing when a given pulse of reactants is injected one could expect the variation of selectivities with the degree of reduction described above to be reversible. In order to check this conclusion, in the second

Fig. 3. (a) Conversion of butene-1 and yields of products as a function of reduction degree of the MoO_3 catalyst. (b) The experiment with intermittent reoxidation of the catalyst with oxygen introduced between pulses of butene-1 shows that on going from MoO_2 to MoO_3 the conversion and yields follow essentially the same pattern as on reduction. It is very difficult, however, to evaluate an extent of reoxidation of the catalyst after each portion of oxygen (marked with arrows) injected, so here the conversion and yields have been plotted as a function of successive number of the pulse of butene-1, rather than, as previously, versus reduction degree.

part of the experiment illustrated in Fig. 3b the reduced catalyst was intermittently reoxidized with oxygen pulses introduced into the microreactor at the reaction temperature, each of them being followed by a series of three pulses (0.6 cm^3) of butene-1. In each series butene-2, butadiene and CO_x were measured after the first and third pulse, and MA after the second one. The changes of the behaviour of the catalyst in the course of reoxidation are in a sense a mirror reflection of the changes observed upon reduction, with all the maxima and minima of yields being also reached simultaneously.

Extensive studies of bismuth molybdate catalysts led to the conclusion [10–12] that in the process of selective oxidation bismuth cations are responsible for the activation of the hydrocarbon molecule, which in the case of olefins consists in abstraction of the α-hydrogen atom and formation of the allylic intermediate. The surface of pure MoO_3 contains a very limited number of sites active in abstraction of hydrogen [13], this role being probably played by lower valent Mo ions. Thus, a monolayer of bismuth ions were deposited on MoO_3 and their contribution as new active sites introduced on the surface of the catalyst, to the reaction network of butene-1 oxidation as function of the degree of reduction of MoO_3 was determined. Results of an experiment, similar to that represented in Fig. 3a, in which successive pulses of butene-1 in oxygen free helium were passed over the Bi^{3+}/MoO_3 catalyst, are shown in Fig. 4. This figure represents only the first half of the experiment in which the degree of reduction x changed from 0 to 0.45. The second half, from 0.5 to 1.0 is symmetrical and similar to that shown in Fig. 3a. In line with the expectations the yield of butadiene (about 20%) at the beginning was much higher than on pure MoO_3

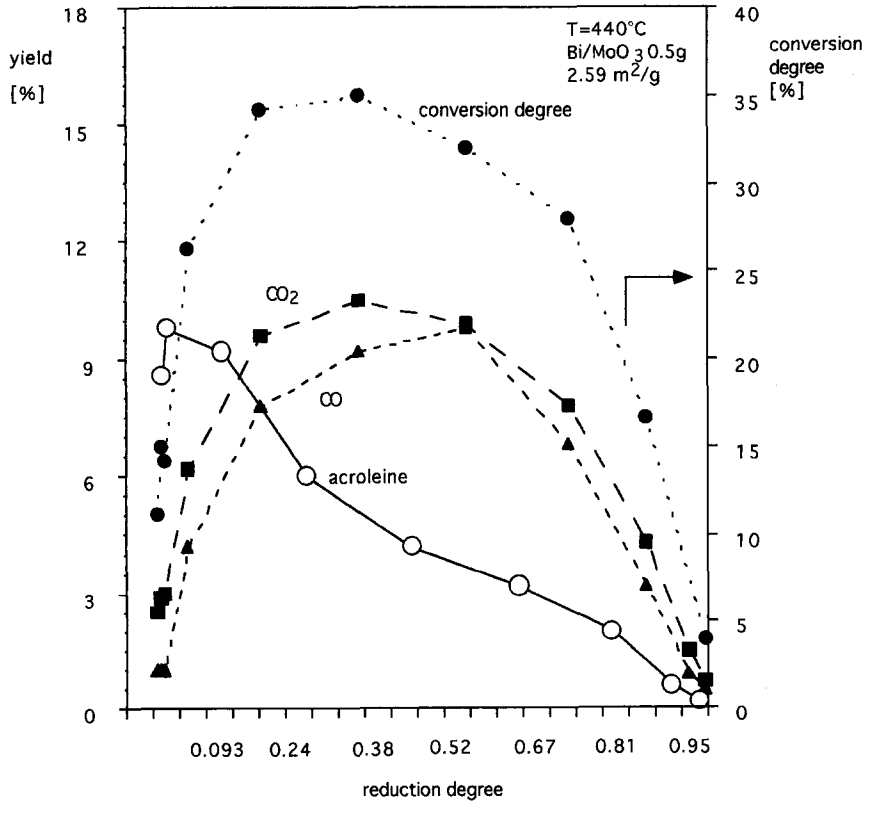

Fig. 5. Conversion of propene and yields of products as a function of reduction degree of the Bi^{3+}/MoO_3 catalyst.

due to the introduction of additional hydrogen abstracting centres in form of Bi^{3+} ions, but the pattern of the changes of selectivity to different products as function of the degree of reduction was similar to that observed in the case of pure MoO_3. The increase of the surface concentration of butadiene accelerated its consecutive transformations into furan and maleic anhydride and hence the rise of their yields was observed. The amount of sites responsible for the total oxidation remained essentially unchanged.

3.2. Reactions of propene

Fig. 5 illustrates the results of experiments in which propene was introduced into the stream of helium passing over the Bi^{3+}/MoO_3 catalyst. Acrolein and $CO + CO_2$ were the only products detected. Conversion amounting to about 35% was considerably lower than in the case of butene-1. The pattern of the changes of the surface concentration of sites, controlling the total oxidation, as function of the degree of reduction, is similar to that observed in the case of butene-1 and is reflected by the dramatic increase of the yield of $CO + CO_2$ until the degree of reduction of about 45% is attained and then equally dramatic decrease of this yield on further reduction to 100%, i.e. the transformation into MoO_2. It is noteworthy, that the yield of acrolein increases with the reduction at the beginning, when the degree of reduction is very small and the yield of total oxidation products remains practically constant at the rather low level, and then starts to decrease, when the yield of the latter rapidly grows, and continues to decrease to zero when the sample approaches the total reduction.

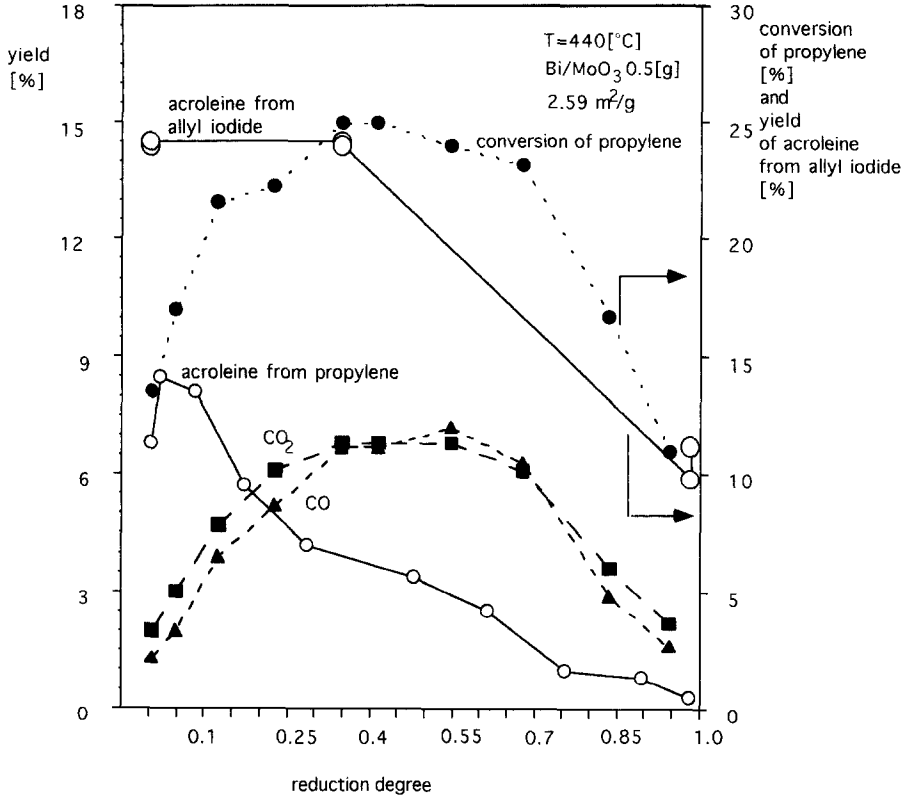

Fig. 6. Conversion of propene and yield of acrolein from allyl iodide as a function of reduction degree of the Bi^{3+}/MoO_3 catalyst.

3.3. Reactions of allyl iodide

Allyl iodide readily decomposes into allyl radical, the strength of the C–I bond in C_3H_5I being 43.5 kcal/mol in comparison to 87.5 kcal/mol for the corresponding bond in propene [13]. When passed through the reactor the first step of the selective oxidation, consisting of formation of the allyl species, is thus facilitated, making possible the examination of active sites, which are necessary for the insertion of nucleophilic oxygen into the activated hydrocarbon molecule in the next step of the reaction [10]. Fig. 6 illustrates the conversion and yields of acrolein and $CO + CO_2$ observed in an experiment, in which the pulses of propene passed over the Bi^{3+}/MoO_3 catalyst as shown in Fig. 5, were at some intervals interchanged with pulses of allyl iodide as marked by bold arrows. The pattern of changes of the yield of acrolein and $CO + CO_2$ from propene is similar to that represented in Fig. 5, whereas the yield of acrolein from allyl iodide is high already at the initial unreduced sample, remains constant until about 40% reduction is attained and then steadily decreases.

3.4. Isomerization of 3,3-dimethylbutene-1

As seen from Fig. 3a pure MoO_3 is mainly a catalyst for isomerization of butene-1 to butene-2, showing some activity in dehydrogenation but practically no activity in oxidation. Isomerization may proceed through the carbocation or allylic mechanism (Scheme 1).

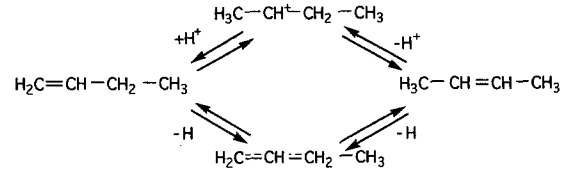

Scheme 1.

In order to find which of these two reaction pathways is operating in the case of MoO_3, its activity in the isomerization of 3,3-dimethylbutene-1 (3,3-DMB-1) into 2,3-dimethylbutene-2 (2,3-DMB-2) and 2,3-dimethylbutene-1 (2,3-DMB-1) was determined. This reaction consists in sigmatropic shift of the methyl group in the carbocation (Scheme 2) and can proceed only when Brønsted acid sites are present at the catalyst surface. The molecule does not contain hydrogen atoms in the α position in respect to the double bond and therefore cannot form allylic species and isomerize along this reaction pathway. It may be therefore used as the probe reaction to measure the concentration of acid sites. Fig. 7 shows the results of a series of experiments, in which several pulses of 3,3-DMB-1 were injected on a fresh sample of MoO_3 catalyst and the yields of the products of its isomerization were measured, then a pulse of pyridine was introduced followed again by pulses of 3,3-DMB-1 injected after different time delays. It may be seen that pyridine which

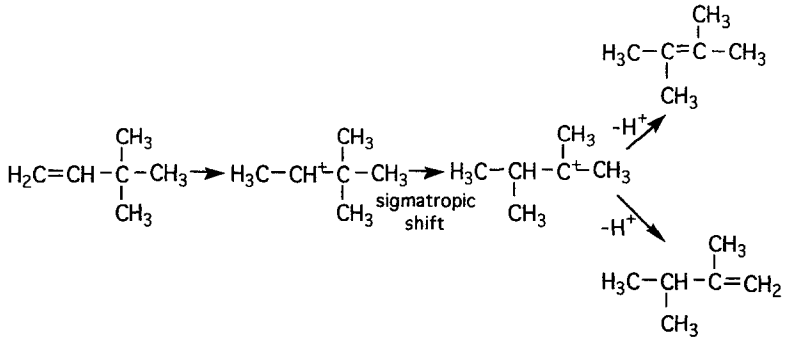

Scheme 2.

is known to adsorb on Brønsted acid sites dramatically decreases the conversion of 3,3-DMB-1 into 2,3-DMB-2. When time delay between the pulse of pyridine and the pulses of 3,3-DMB-1 is prolonged, pyridine becomes desorbed from the sample by the stream of the He carrier gas and the isomerization activity increases back to its initial value. This indicates that the isomerization of 3,3-DMB-1 proceeds indeed through the formation of carbocation by interaction with proton acid sites, and that the catalytic activity of MoO_3 in isomerization is due to the presence of these sites. In the next series of experiments the isomerization of 3,3-DMB-1 was measured on samples A, B and C of the catalyst representing different stages of its reduction. It should be remembered that it is the conversion of 3,3-DMB-1 to 2,3-DMB-2 and 2,3-DMB-1 i.e. their yields which are the measure of the isomerizing activity of the catalyst and not the total conversion of 3,3-DMB-1 which includes its transformations along other reaction pathways as, e.g. oligomerization, cracking etc. These processes lead to the deposition of coke, which probably is the cause of the decrease of the isomerization with the number of pulses, visible in Fig. 8A and Fig. 8B. Comparison of the yields of 2,3-DMB-2, extrapolated to the initial pulse, shown in Fig. 8A, Fig. 8B and Fig. 8C, clearly indicate that the amount of acid sites or their strength diminishes on reduction and that this effect may be responsible for the decrease of the selectivity to products of isomerization of butene-1 on reduction of MoO_3 illustrated in the left part of Fig. 3a. Obviously, this cannot explain the rise of the isomerization in the right part of Fig. 3a because the surface acidity of MoO_2 as indicated by the yield of 2,3-DMB-2 in Fig. 8C is very low. It must be thus due to the onset of the second reaction pathway through an allylic intermediate.

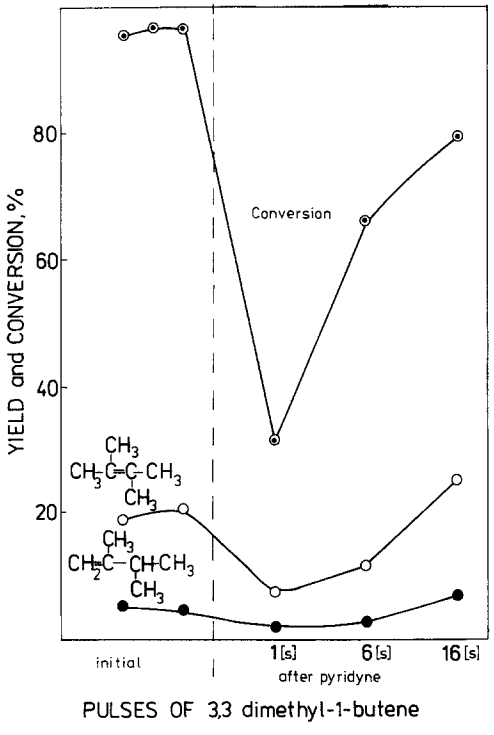

Fig. 7. The poisoning effect of preadsorbed pyridine on the conversion of 3,3-DMB-1 on MoO_3.

3.5. Isomerization of 2,3-DMB-2

In order to determine the ability of the surface exposed in the course of the reduction of MoO_3 to MoO_2 to generate allylic species the isomerization of 2,3-DMB-2 to 2,3-DMB-1 was used as the probe reaction. This process may proceed either through the formation of the carbocation or the allylic intermediate (Scheme 3).

As the 2,3-DMB-2 molecule contains 12 allylic hydrogens the probability of the second reaction pathways is very high and it can be expected to be dominant. Fig. 9 shows a series of experiments in which pulses of 2,3-DMB-2 were passed over the MoO_3 catalyst and the yield of 2,3-DMB-1 was measured. Then a pulse of pyridine was injected to poison the proton acid sites and then pulses of 2,3-DMB-2 were again introduced after different time delays. It may be seen that indeed the yield of 2,3-DMB-1 is not influenced by addition of pyridine although the acid sites are poisoned as indicated by the dramatic decrease of conversion in other acid type side reactions. It may be thus con-

cluded that in the case of MoO_3 catalysts the isomerization of 2,3-DMB-2 proceeds mainly through the allylic pathway and may be used as a probe reaction to detect the presence of sites activating the hydrocarbon molecules by abstraction of hydrogen and formation of an allylic species.

The yields of 2,3-DMB-1 obtained as the result of isomerization of 2,3-DMB-2 on MoO_3 catalyst which has been reduced to different

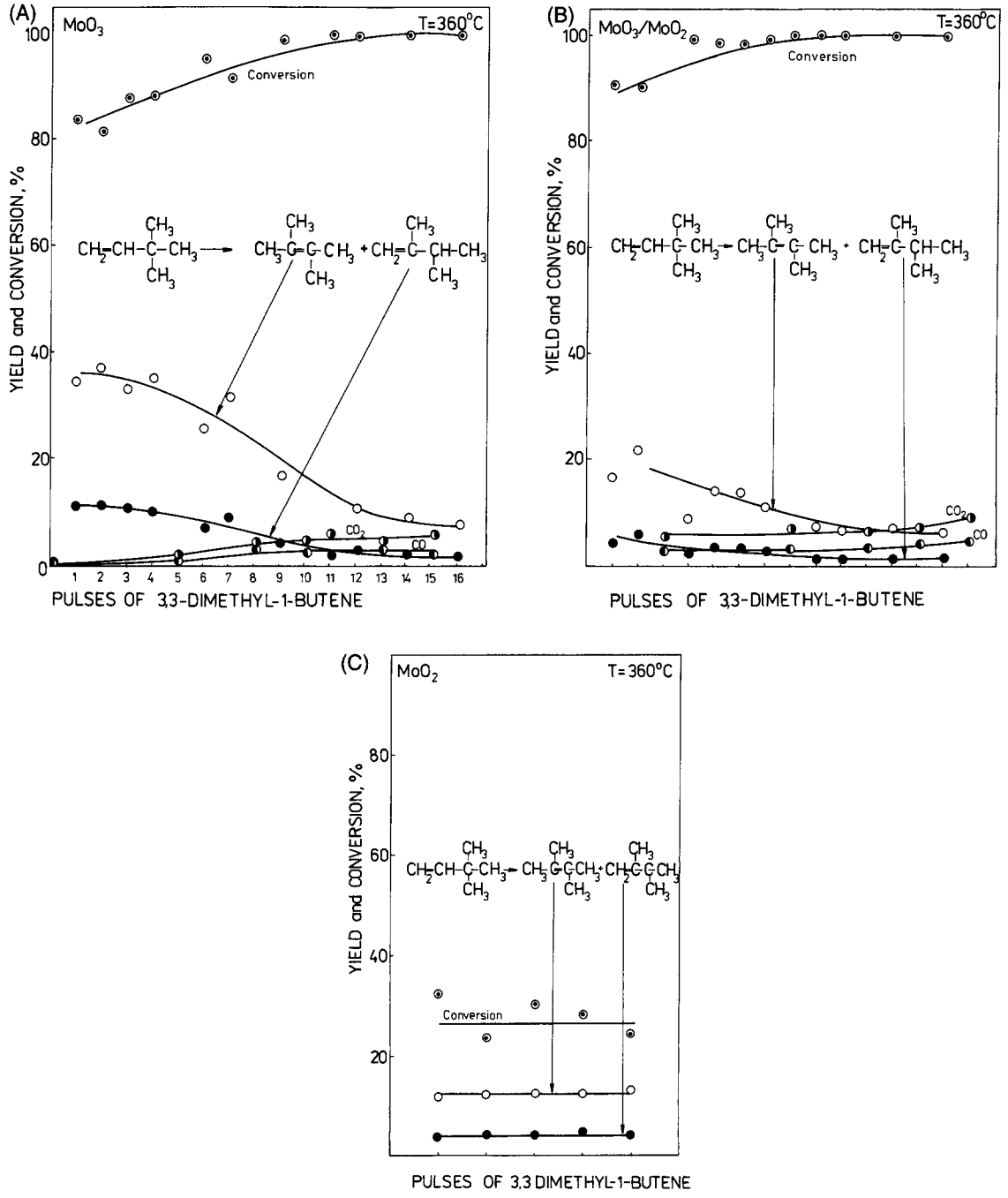

Fig. 8. Conversion of 3,3-DMB-1 as a probe of Brønsted acidity of MoO_3: (A) fresh sample; (B) sample at a reduction degree of ~ 0.5; (C) fully reduced sample.

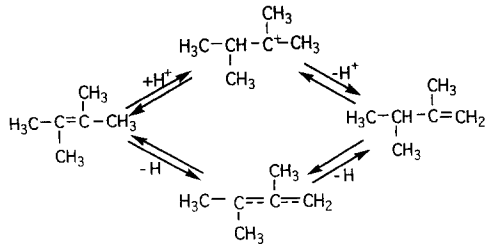

Scheme 3.

degrees in the flow of hydrogen before each series of 2,3-DMB-2 pulses are illustrated in Fig. 10. It may be seen that the steady-state yield attained in each series is independent of the degree of reduction what may be taken as an indication that the activity of sites generating the allyl species from a hydrocarbon molecules does not change on reduction of the catalyst. Apparently the increasing activity in isomerization of butene-1 observed in the right part of the experiment shown in Fig. 3a may be explained by assuming that the allylic mechanism of isomerization is taking over the carbocation mechanism and on MoO_2, which shows no surface acidity, this process is proceeding via an allylic intermediate.

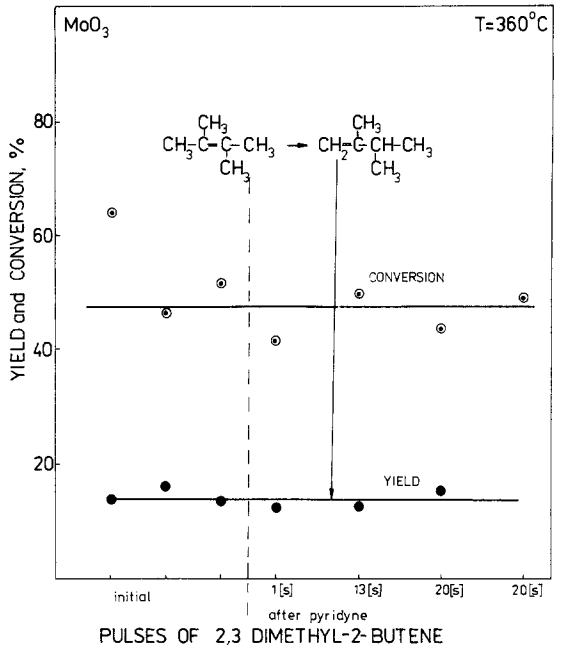

Fig. 9. Preadsorbed pyridine does not affect production of 2,3-DMB-1 from 2,3-DMB-2 on MoO_3 catalyst.

3.6. XRD analysis

The XRD analysis showed that the initial catalyst (sample A) was pure MoO_3 and at the

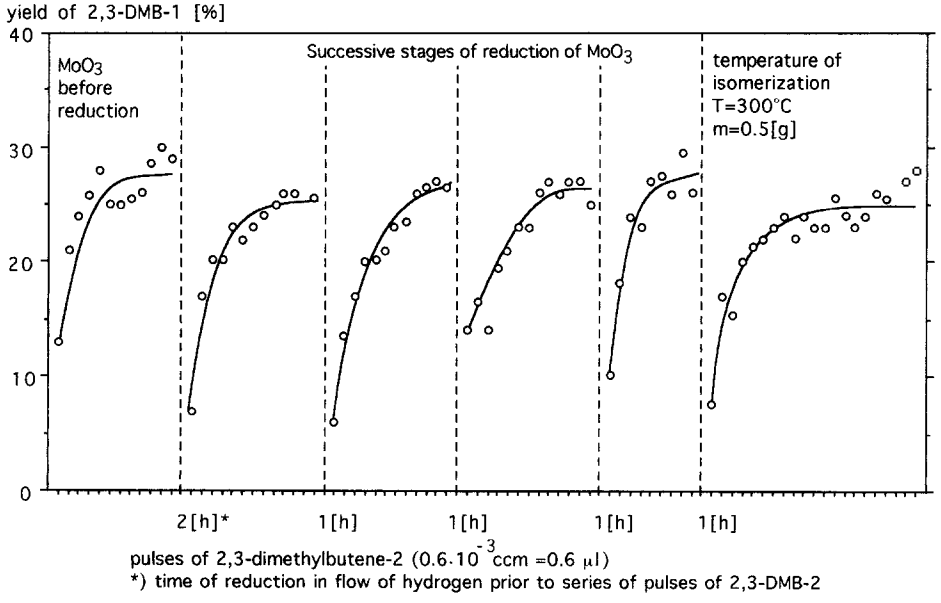

Fig. 10. Conversion of 2,3-DMB-2 as a probe of allylic activation on the MoO_3 catalyst.

end of the reduction (sample C) only the XRD-pattern of MoO_2 was visible, the mixture of the two phases being observed in the middle of the experiment (sample B) at the point corresponding to the extreme on the selectivity curves. At this point the XRD shows only the presence of a mixture of MoO_2 and MoO_3. The surface area of the sample did not change significantly throughout the experiment, being 2.59 $m^2\ g^{-1}$, 3.1 $m^2\ g^{-1}$ and 3.02 $m^2\ g^{-1}$ for samples A, B and C, respectively. It is noteworthy that neither on reduction nor in the course of reoxidation were any reflections observed of intermediate oxide phases, in particular of Mo_4O_{11} reported in [14–17].

3.7. Photoelectron spectra

Photoelectron spectra of Mo3d electrons for samples A, B and C are shown in Fig. 11A, Fig. 11B and Fig. 11C, respectively. The range of binding energies of Mo3d electrons in the spectrum of the initial sample (Fig. 11A) shows the presence of a doublet at 233.5 eV and 236.6 eV characteristic for Mo^{6+} ions in oxide matrices [18–22]. The separation between the two components of the doublet is 3.2 eV in very good agreement with the values reported in the literature [18–22]. The range of binding energies of oxygen photoelectrons shows a peak at 531.3 eV typical for lattice oxygen ions in transition metal oxides. Three doublets appear in the Mo3d range of the spectrum registered for the partially reduced sample B, one having the maxima at 233.5 eV and 236.6 eV indicating the presence of Mo^{6+} ions, the second with the maxima at 231.7 and 234.8 eV, and the third showing maxima at 230.1 and 233.2 eV. The same three doublets are visible in the spectrum of the sample C after completing the catalytic experiment, but the third doublet is now dominating. In the spectral range of O1s photoelectrons a new peak appears at 532.8 eV, its intensity increasing with the progress of the reduction. It may be assigned to OH^- groups. Some extra features visible on the left side of the Mo3d and O1s

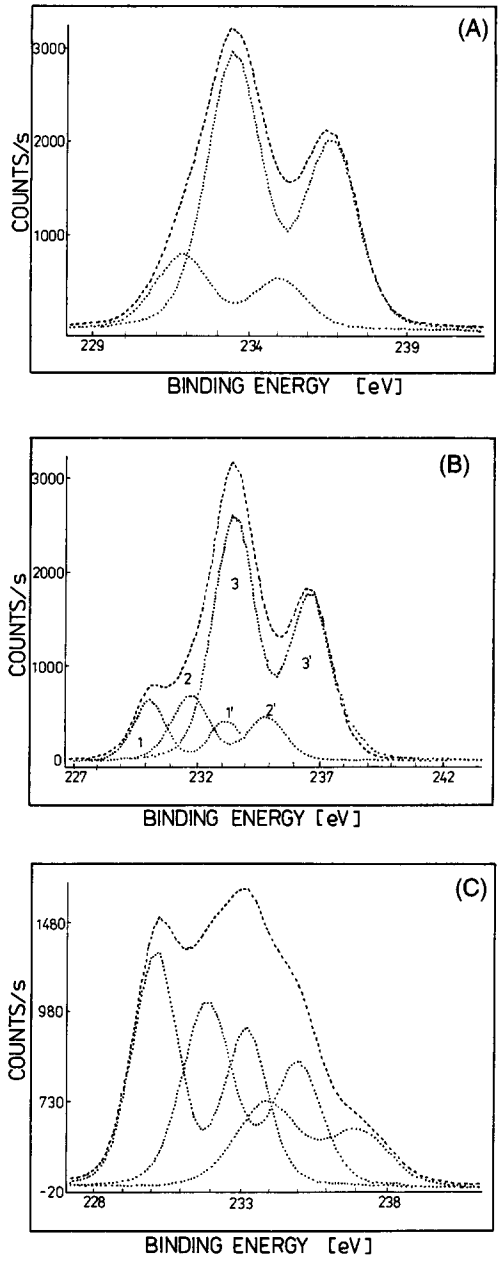

Fig. 11. Photoelectron spectra of Mo3d electrons for (A) fresh sample, (B) sample at reduction degree of ~0.5, and (C) fully reduced sample.

peaks may be indicative of the differential charging of the grains due to the limited conductivity of MoO_3.

For a series of simple compounds which are build of similar coordination polyhedra of the given cation and differ only in the valence state

of the cation, i.e. in the way in which the coordination polyhedra are linked together, it may be assumed that a linear dependence exists between the binding energy of the core electrons and the valence state. This dependence can be used for the assignment of the three different doublets obtained on reduction of MoO_3 [23,24]. Two points are fixed: the position of Mo^{6+} ions and the position of metallic molybdenum. Analysis of such dependence shows that the doublet at 231.7 and 234.8 eV should be assigned to molybdenum ions of apparent oxidation number +4, and the doublet at 230.1 and 233.2 eV to ions of apparent oxidation number +2. It should be borne in mind the true charge on the metal ion, which determines the electron binding energy measured by XPS, is dependent on the entire balance between the ionicity and the covalency of the oxide and the existence of metal–metal bonds and is not equal to the rather artificially constructed oxidation number. After contacting MoO_3 with hydrogen or the hydrocarbon oxygen vacancies are generated by removal of the lattice oxygen ions, an rearrangement of the initially corner linked metal oxygen octahedra into an arrangement of edge linked octahedra takes place, resulting in the formation of a shear plane. The two electrons for each vacancy become localized at the bonding orbital formed between two adjacent Mo^{6+} ions, which appear as Mo^{4+}. On further reduction, nucleation of MoO_2 lattice takes place. It should be remembered at this point that structural analysis of the transition metal dioxides MO_2 crystallizing in the rutile-type structure has shown that two different metal–metal distances are observed in these lattices: successive pairs of metal atoms in a string of edge-sharing octahedra are brought alternately closer together and further apart [25]. The distances between adjacent metal atoms are so short that they indicate the formation of multiple metal–metal bonds between central atoms of edge-sharing octahedra. The two Mo^{4+} form a double bond and appear in XPS spectrum as having the apparent oxidation number +2. Indeed, quantum chemical calculations of clusters of MoO_6, WO_6 and ReO_6 octahedra, carried out by means of SCF-Xa method showed to be consistent with the results of XPS studies, indicating the formation of single and double metal–metal bonds [26,27] and the shift of formal oxidation number. It is noteworthy that the appearance of discrete Mo^{5+} ions in the course of reduction of MoO_3 was ruled out because of the very low, positive values of magnetic susceptibility observed for all intermediate compounds [28]. The presence of very small amounts of Mo^{5+} ions was detected by EPR spectroscopy in MoO_3 reduced to a small degree [29,30]. It may be thus concluded that our sample B contained domains of MoO_3 with the shear planes and embedded crystallites of MoO_2, whereas sample C contains MoO_2 and the rest of the disordered framework of shear structures.

3.8. IR spectra

Fig. 12 illustrates the IR spectra of the three samples. The spectrum of sample A is typical for MoO_3 with bands at 996 cm^{-1}, 862 cm^{-1}, 825 cm^{-1} and 570 cm^{-1} corresponding to the stretching vibrations of terminal Mo = O groups, Mo–O–Mo bridges between ribbons and Mo–O–Mo bridges within the ribbons, respectively. In the partially reduced sample B the matrix of MoO_3 is retained, the reduction being reflected in the increased background absorption well

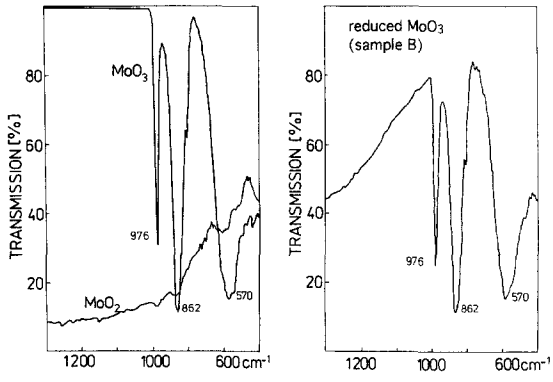

Fig. 12. IR spectra of fresh sample (MoO_3), fully reduced sample (MoO_2), and sample at a reduction degree of ~0.5.

visible in the range of higher wavenumbers. The MoO_3 bands disappear completely from the spectrum of sample C which becomes practically featureless in this spectral range.

4. Discussion

Mechanism of the reduction of MoO_3 in different media (vacuum, hydrogen, CO, hydrocarbons) has been extensively studied by different methods. Ample experimental evidence seems to indicate that depending on the conditions of the reduction there are basically two different pathways of the reaction:

(a) Reduction starts with the formation of oxygen vacancies, which aggregate into discs and by crystallographic shear form shear planes. When the concentration of shear planes grows they become ordered and form the Magnelli phases, Mo_nO_{3n-1}. At higher temperatures the structure disintegrates into crystallites of Mo_4O_{11}, which then transforms into MoO_2 [31].

(b) Reduction starts with the formation of oxygen vacancies at (010) plane by adsorption of hydrogen on terminal oxygen atoms [32] and desorption of water along the [101] series of octahedra. This results in the formation of a layer of MoO_2 structure. Reduction layer by layer and collapse of the layers as described below leads to the formation of MoO_2 [33,34].

The conditions, in which these mechanisms were observed, are summarized in Table 1. The data presented in Table 1 indicate that in mild conditions nucleation of the domains of MoO_2 within the lattice of MoO_3 takes place, which expand with the advancing degree of the reduction.

A detailed study of the course of reduction using XRD and HREM leads to the conclusion that the $MoO_3 \rightarrow MoO_2$ transformation is topotactic [33,34]. In the two-layer sheets of MoO_3 parallel to (010) crystal planes each layer considered separately is built of MoO_6 octahedra linked through their corners. Similarly, the (100), (210), (41) and (201) planes of MoO_2 is also composed of MoO_6 octahedra, connected through corners [34]. When [010] axis of MoO_2 is put collinearly to [101] axis of MoO_3 the superposition of both planes is almost perfect, and their respective symmetry is identical (Fig. 13). On the other hand many observations show that the migration of hydrogen, hydroxyl groups or even water molecules in MoO_3 occurs preferentially along the pathway parallel to the [010] direction and the experimental activation energy of the MoO_3/MoO_2 interface displacement in the course of reduction is compatible with a

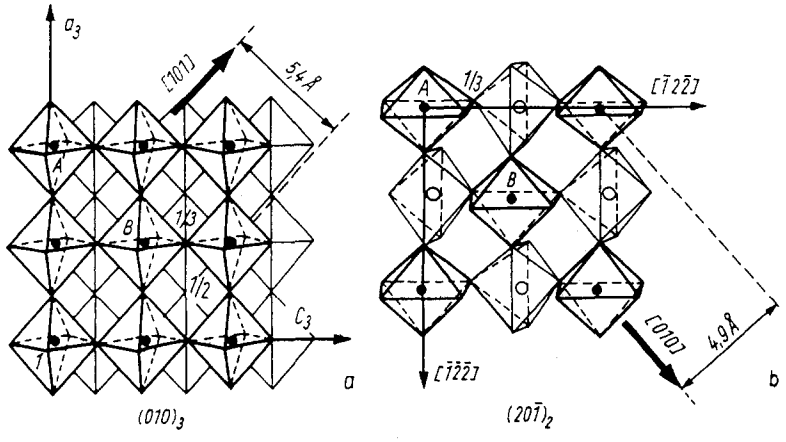

Fig. 13. The (010) crystal plane of MoO_3, denoted as $(010)_3$, and the $(20\bar{1})$ plane of MoO_2 denoted as $(20\bar{1})_2$ (after [33]).

Table 1
Summary of mechanisms of reduction of MoO_3 at different conditions

Technique	Conditions	Mechanism observed	Ref.
HREM	UHV	$MoO_3 \rightarrow CS \rightarrow MoO_2$	[40]
Conv. beam ED	H_2	$MoO_3 \rightarrow MoO_{3-x}(OH)_x$	[36]
TG, XRD	$H2/H_2O$, 300–400°C	$MoO_3 \rightarrow MoO_2$ vacuum pretreatment $MoO_3 \rightarrow Mo_4O_{11}$ nitrogen pretreatment	[14]
HREM, XRD	Dry H_2, 450°C	$MoO_3 \rightarrow$ topotactic $\rightarrow MoO_2$	[33]
RHEED, AES	H_2, 20–450°C	$MoO_3 \rightarrow$ topotactic $\rightarrow MoO_2$	[34]
HREM	H_2/He, 100–400°C	$MoO_3 \rightarrow CS \rightarrow MoO_2$	[41,42]
XRD	H_2	$MoO_3 \rightarrow Mo_4O_{11} \rightarrow MoO_2$	[15]
LEED, XPS, UPS, EELS	UHV, 20–600°C, Ar^+ sputtering	$MoO_3 \rightarrow CS \rightarrow MoO_2$	[18]
EMD	UHV	$MoO_3 \rightarrow CS$	[43]
XRD	Toluene + NH_3 + O_2 + N_2, 450°C	$MoO_3 \rightarrow MoO_2$, Mo_4O_{11} formed on reoxidation	[16]
XRD, Gravimetry	H_2, 460–540°C	$MoO_3 \rightarrow Mo_4O_{11} \rightarrow MoO_2$	[17]
XPS, LRS	H_2, N_2, 350–730°C	$MoO_3 \rightarrow CS \rightarrow MoO_2$	[44]
XRD, IR, XPS	H_2, propene, butene, 440°C	$MoO_3 \rightarrow MoO_2$	This work

migration energy of anionic vacancies along the [010] direction [35]. A synchronous and differentiated movement of oxygen atoms in MoO_3 layers may be now envisaged, consisting – as shown in Fig. 14 – of slipping of the two consecutive layers along 1/2[001] direction in MoO_3 followed by collapse along 1/7[010] direction, which results in the formation of a structure in which all the oxygen atoms are common to three octahedra as in MoO_2. When performed layer by layer – it will transform the initial MoO_3 structure into MoO_2 lattice. It should be noticed that the removal of all the oxygens bordering the (010) layers and connected to a single Mo atom results in the MoO_2 composition. The water molecules or hydroxyl groups formed diffuse easily in the structural holes of MoO_2 along [100] direction. It may be mentioned that Bursill et al. [36] consider the MoO_3 crystal to be built of MoO_2 layers and oxygen according to the sequence:

$$MoO_2\text{-}O_2\text{-}MoO_2\text{-}MoO_2\text{-}O_2\text{-}MoO_2$$

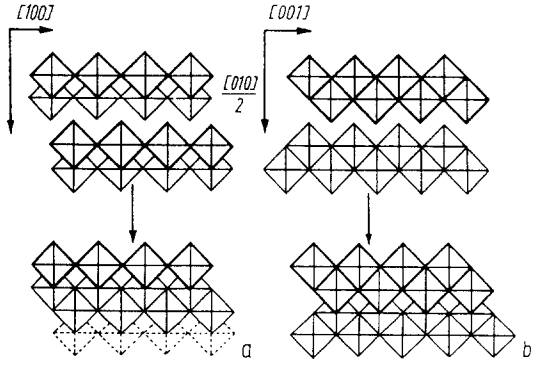

Fig. 14. Slipping of two adjacent MoO_3 layers along 1/2[001] direction followed by collapse along 1/7[010] viewed along (a) [001] direction and (b) [100] direction (after [33]).

It should, however, be borne in mind that our earlier studies of the reduction of MoO_3 by hydrogen and propene, carried out by "in situ" EPR [37], as well as recent results of the measurements of Raman spectra after ^{18}O exchange with MoO_3 during the oxidation of butene [38] clearly indicate that the process of reduction of the MoO_3 layer proceeds through the removal of oxygen atoms from Mo–O–Mo bridges linking the ribbons of MoO_6 octahedra in the [100] direction.

The observation that the IR spectrum of our MoO_3 catalyst after about 45% reduction is almost identical to that of the initial sample except for the increase of the background absorption is in line with the mechanism shown in Fig. 14. Also the results of XPS studies indicate that the reduction proceeds through a continuous change of the valence state of Mo ions from Mo^{6+} to Mo^{4+}.

The change of valency of Mo ions and the structural changes occurring in the course of the

reduction have a profound influence on the surface properties of the catalyst. They are summarized in Fig. 15. The results of the measurements of the changes of activity in isomerization of 3,3-dimethylbutene-1 as function of the degree of reduction, which can be considered as the measure of the surface concentration and strength of acid sites, show that the surface acidity decreases continuously to disappear after the transformation into MoO_2. On the contrary, the surface concentration of sites abstracting hydrogen atoms, as indicated by the activity in isomerization of 2,3-dimethylbutene-1, remains practically unchanged. The ability of the surface to perform the addition of nucleophilic oxygen, measured by the transformation of allyl radicals into acrolein, which is characteristic for MoO_3 surface remains at first constant, but then, on shrinking of the domains of MoO_3 and growth of those of MoO_2 decreases. The only property, which passes through an extreme, is the ability to generate the electrophilic oxygen. At first it considerably grows with the increasing degree of reduction, passes through a maximum when the degree of reduction of about 45–50% has been attained and then decreases almost to zero when the reduction is completed. It must be emphasized that the reactions of butene were studied in the absence of the gas phase oxygen. Because the electrophilic attack on the butene molecule, resulting in its total oxidation to CO

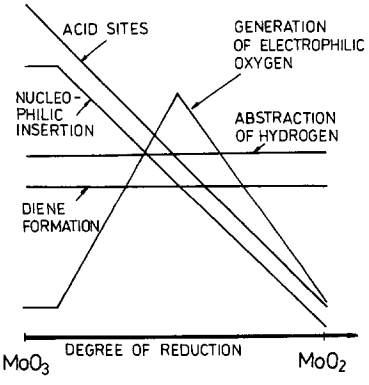

Fig. 15. Schematic representation of MoO_3 catalytic functions changed upon the reduction of the catalyst.

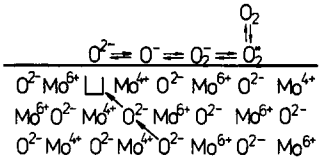

Fig. 16. Equilibrium between the lattice and the gas-phase oxygen.

and CO_2 competes with the parallel reaction of butene isomerization (see Fig. 3a), the pattern of the changes of isomerization with the degree of reduction is inverse to that of the total oxidation to $CO + CO_2$. A question may be raised as to which is the reason of the increasing activity of the surface lattice oxygen of MoO_3 in the course of its reduction, although the reverse behaviour could be expected: MoO_3 is a much stronger oxidant than MoO_2.

MoO_3 is a non-stoichiometric oxide, whose lattice components are in equilibrium with the gas phase. Its intrinsic defect structure consists of oxygen vacancies:

$$O_O \rightarrow V_O + \frac{1}{2}O_2$$

$$V_O \rightarrow V_O^+ + e^-$$

$$V_O^+ \rightarrow V_O^{2+} + e^-$$

At each temperature and oxygen pressure an equilibrium is established between oxygen atoms in the lattice and oxygen molecules in the gas phase. Because it is a dynamic equilibrium, a continuous process of evolution of oxygen from the surface and its reabsorption by the surface must take place, as shown in Fig. 16, the surface being always populated by transient oxygen species O^-(surf), O_2^-(surf) and O_2(surf), which are strongly electrophilic species and are responsible for the total oxidation of hydrocarbon molecules. The surface coverage of MoO_3 by these species depends on temperature, pressure of oxygen in the gas phase and chemical potential of oxygen in the lattice, i.e. on the position of the Fermi level in the solid. When MoO_3 becomes exposed to the reducing agent, isolated oxygen vacancies are at first formed

and the electrons released in this process become localized on Mo^{6+} ions reducing them to the corresponding number of Mo^{4+} ions. These ions are situated at the surface and play the role of catalytic sites, activating the hydrocarbon molecules by abstraction of hydrogen. This is clearly visible in the case of the oxidation of propene, presented in Fig. 5. At the beginning of the experiment, when the degree of reduction is very small, its increase causes a considerable increase of the oxidation of propene to acrolein. As the rate determining step is the activation of propene, it can be concluded that surface reduction generated new active sites accelerating this step. It is noteworthy that in this range the total oxidation of propene to $CO + CO_2$ is practically constant. When a certain degree of reduction has been attained, rapid increase of the total oxidation is observed. It can be assumed that the onset of this increase of total oxidation is related to the nucleation of the domains of MoO_2 in the matrix of MoO_3. When such domains appear, the interface is formed between MoO_3 and MoO_2 regions of the crystallites and a contact potential must appear at this interface. The value of work function of MoO_2 is smaller than that of MoO_3 and consequently an electron transfer will take place from MoO_2 to MoO_3, charging negatively the surface of MoO_3, as shown in Fig. 17. Due to bending of energy bands at the interface, the conductivity band will shift at the surface of MoO_3 below the Fermi level so that the low-lying levels in this band will be occupied by electrons. The increased negative charge would lower the binding energy of oxide ions at the surface of MoO_3, which would result in the increase of the population of the surface with transient electrophilic oxygen species and hence in acceleration of the total oxidation. This process will continue with the expansion of the MoO_3/MoO_2 interface until a maximum is attained and then should decrease when MoO_3 is more and more consumed.

If such a mechanism is indeed operating, the effect should be also produced by mechanical

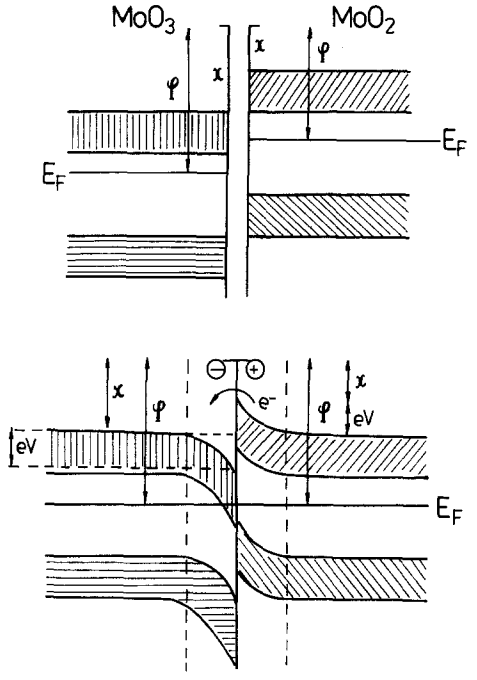

Fig. 17. Because of difference in work function, a contact potential appears at the MoO_3/MoO_2 interface, and an electron transfer from MoO_2 to MoO_3 charges negatively the surface of the latter.

mixing of the two oxides and should depend on the grain size and on the degree of intergranular contacts. In order to check this conclusion, mechanical mixtures of MoO_3 and MoO_2 were prepared after different pretreatment in order to change the grain size. The results shown in Fig. 18 clearly demonstrate that the activity in total oxidation of butene by lattice oxygen of MoO_3 dramatically depends on the way this oxide is mixed with MoO_2. It is noteworthy that the activity of the mechanical mixture containing 50% MoO_3 and 50% MoO_2 in total oxidation of butene was comparable to that observed after attaining the degree of about 50% reduction of MoO_3 in the experiment in which it has been reduced "in situ" by pulses of butene (Fig. 19). When, however, this mechanical mixture was then exposed to reducing pulses of butene, the activity in total oxidation increased further and attained a maximum at the degree of reduction, corresponding to about 80% of MoO_2. At that

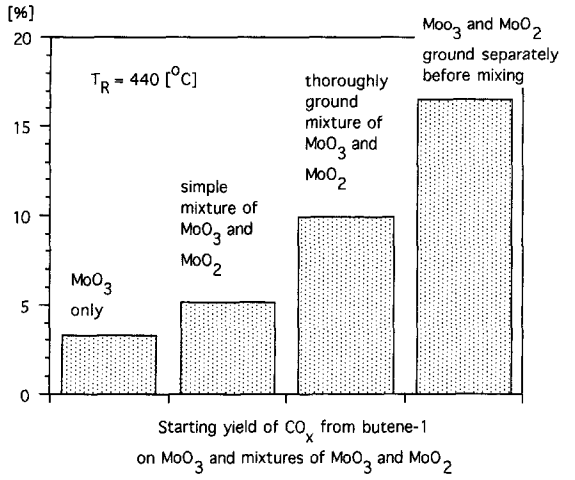

Fig. 18. Formation of CO_x from butene-1 on mechanical mixture of MoO_3 and MoO_2.

point the activity of the reduced mechanical mixture in total oxidation was much higher than the activity of the catalyst obtained by reduction of MoO_3 to the same level of 80%. This result strongly supports the proposed model. Namely, the reduction of the 50% MoO_3/50%MoO_2 mechanical mixture generates new interfaces within the grains of MoO_3 and hence increases the total number of transient oxygen species, active in total oxidation.

In order to further confirm this mechanism, measurements of the potential of MoO_3/MoO_2 powder electrodes were carried out. When equilibrium has been established the potential measured by the electrode Pt2 inserted in the powder should be equal to

$$E_{exp} = E_F(SCE) - E_F(MoO_3/MoO_2)$$

and it should be thus indicative of the position of Fermi level in the powder mixture. The reduced MoO_3 must contain a very high concentration of surface states. The capture of charge on these surface states may cause the surface Fermi level to shift toward the surface states energy so that the Fermi level becomes controlled entirely by the surface states independently of its position in the bulk [39]. Thus, one could expect that the potential of the powder electrode will continuously decrease with the

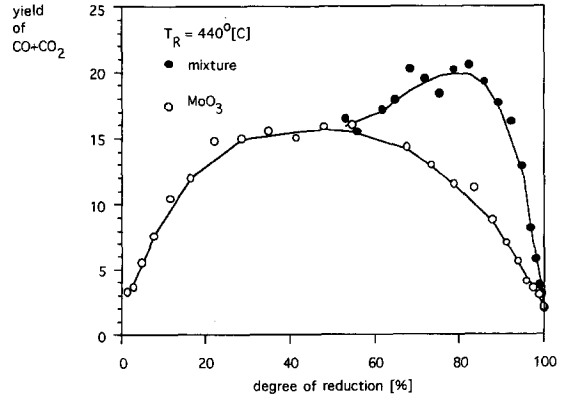

Fig. 19. Formation of CO_x from butene-1 as a function of reduction degree of MoO_3 and the mechanical mixture of MoO_3/MoO_2.

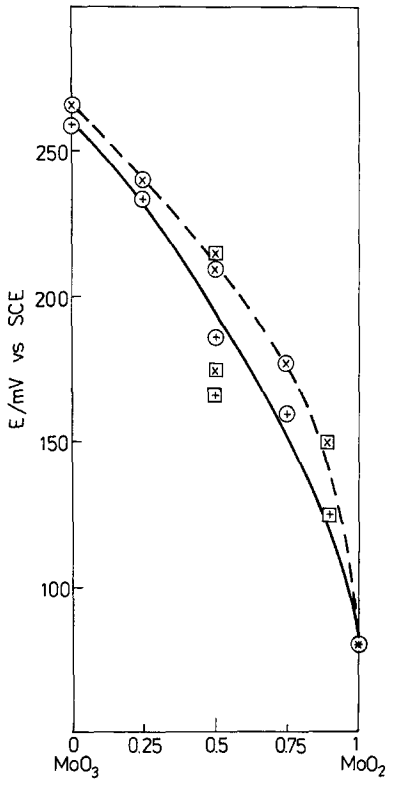

Fig. 20. Potential of the powder MoO_3/MoO_2 electrodes as a function of MoO_2 content in the mixture. Solid line represents the potential measured in the powder; dashed line, in the solution. Circles refer to mechanical mixtures of MoO_3 and MoO_2, squares refer to samples of the catalyst at the corresponding stage of reduction.

expanding MoO_3/MoO_2 interfaces from the value characteristic to MoO_3 to the value observed for MoO_2. Results presented in Fig. 20 seem to confirm this conclusion. It is noteworthy that the potentials measured for preparations obtained by "in situ" reduction of MoO_3 with butene-1 are similar to those measured for the mechanical mixtures of MoO_3 and MoO_2 of the corresponding compositions indicating similar electronic structures of the surface which apparently determines their catalytic properties.

References

[1] J. Haber, in E.R. Braitwaite and J. Haber, Editors, Molybdenum: An Outline of its Chemistry and Uses, Elsevier, Amsterdam, 1994, p. 477.
[2] J. Haber, Stud. Surf. Sci. Catal., 72 (1992) 279.
[3] J.B. Goodenough, in H.E. Barry and P.C. Mitchell, Editors, Proc. Climax 4th Intern. Conf. Chemistry and Uses of Molybdenum, Climax Molybdenum Co., Ann Arbor, MI, 1982, p. 1.
[4] K. Brückman, R. Grabowski, J. Haber, A. Mazurkiewicz, J. Sèoczyáski and T. Wiltowski, J. Catal., 104 (1987) 71.
[5] K. Brückman, J. Haber and T. Wiltowski, J. Catal., 106 (1987) 188.
[6] J.C. Volta, J.M. Tatibouet, C. Phichithul and J.E. Germain, Proc. 8th Intern. Congr. Catal., Berlin, 1984, Verlag Chemie-Dechema, Frankfurt, 1984, Vol. 4, p. 457.
[7] A. Guerrero-Ruiz, J. Massardur, D. Duprez, M. Abon and J.C. Volta, in J.M. Phillips and N. Ternan, Editors, Proc. 9th Int. Congr. Catal., Calgary, 1988, The Chemical Institute of Canada, Ottawa, 1988, p. 1601.
[8] J. Haber and E. Serwicka, Polyhedron, 5 (1986) 107.
[9] T.S. Oyama, Bull. Chem. Soc. Jpn., 61 (1988) 2585.
[10] B. Grzybowska, J. Haber and J. Janas, J. Catal., 49 (1977) 150.
[11] R.K. Grasselli and J.D. Burrington, Adv. Catal., 30 (1981) 133.
[12] J. Haber, Proc. 8th Intern. Congr. Catal., Berlin, 1984, Verlag Chemie-Dechema, Frankfurt, 1984, Plenary Lectures, Vol. 1, p. 85.
[13] S.W. Benson, Thermochemical Kinetics, Wiley, New York, 1968, p. 215.
[14] R. Burch, J. Chem. Soc., Faraday Trans. 1, 74 (1978) 2982.
[15] A. Ueno, Y. Kotera, S. Okuda and C.O. Bennett, Proc. Climax 5th Int. Conf., 1982, p. 250.
[16] A. Anderson and S. Hansen, J. Solid State Chem., 75 (1988) 225.
[17] J. Stoczyáski and W. Bobinski, J. Solid. State Chem., 92 (1991) 420; 92 (1991) 436.
[18] L.E. Firment and A. Faretti, Surf. Sci., 129 (1983) 155.
[19] A. Cimino and B.A. De Angelis, J. Catal., 36 (1975) 11.
[20] T.H. Fleisch and G.J. Mains, J. Chem. Phys., 76 (1982) 780.
[21] W.E. Swartz, Jr. and D.M. Hercules, Anal. Chem., 43 (1971) 1774.
[22] B. Grzybowska, J. Haber, W. Marczewski and L. Ungier, J. Catal., 42 (1976) 327.
[23] J. Haber, W. Marczewski, J. Stoch, L. Ungier, Ber. Bunsenges Phys. Chem., 79 (1975) 970.
[24] J. Haber, J. Less Common Met., 54 (197) 243.
[25] A.F. Wells, Structural Inorganic Chemistry, Oxford University Press/Clarendon Press, Oxford, 1962.
[26] E. Broctawik, A. Foti and V.H. Smith, Jr., J. Catal. 62(1980) 185.
[27] E. Broctawik, J. Haber and L. Ungier, J. Phys. Chem. Solid, 42 (1981) 203.
[28] R.L. McCormic and G.L. Schrader, J. Catal., 113 (1988) 529.
[29] E. Serwicka, J. Solid State Chem., 51 (1984) 300.
[30] K. Dyrek, M. Tabanowska, J. Chem. Soc., Faraday Trans., 87 (1991) 1003.
[31] K. Hermann, A. Michalak and M. Witko, Catal. Today, in press.
[32] P.L. Gai-Boyes, Catal.-Rev. Sci. Eng., 34 (1992) 1.
[33] O. Bertrand and L.C. Dufour, Phys. Status Solidi (a), 60 (1980) 507.
[34] O. Bertrand, L.C. Dufour and N. Floquet, Surf. Sci., 147 (1984) 396.
[35] M.J. Kennedy, S.C. Bevan, J. Less Common Met., 36 (1974) 23.
[36] L.A. Bursill, W.C.T. Dowell, P. Godman and N. Tate, Acta Crystallogr. A, 34 (1974) 296.
[37] J. Haber, ACS Symp. Ser., 279 (1985) 3.
[38] T. Ono, H. Numata and N. Ogata, private communication, 1995.
[39] S.R. Morrison, in N.B. Hannay, Editor, Treatise on Solid State Chemistry, Vol. 6B, Plenum Press, New York, 1976, p. 203.
[40] L.A. Bursill, Acta Crystallogr. A, 28 (1972) 187.
[41] P.L. Gai, Philos. Mag. A, 43 (1981) 841.
[42] P.L. Gai and P.A. Labun, J. Catal., 94 (1985) 79.
[43] J.M. Dominuez-Esquivel, S. Fuentes-Moyado, G. Diaz-Guerrero and A. Vazquez-Zavala, Surf. Sci., 175 (1987) L701.
[44] P.A. Spevack and N.S. McIntyre, J. Phys. Chem., 96 (1992) 9029.